Flexural Fillet Geometry Optimization for Design of Force Transducers used in Aeronautics Testing

Keith C. Lynn*

Genevieve Dixon†

NASA Langley Research Center, Hampton, Virginia 23681

Force transducer designs used in the ground testing aeronautics community have seen minimal change over the last few decades. With increased focus on data quality and long-term performance capabilities over the life of these instruments, it is critical to investigate new methods that improve these designs. One area of focus in the past few years at NASA has been on the design of the flexural elements of traditional force balance transducers. Many of the heritage balances that have been heavily used over the last few decades have started to develop fatigue cracks. The recent focus on the flexural design of traditional single-piece force balances revolves around the design of these elements such that stress concentrations are minimized, with the overall goal of increasing the fatigue life of the balance. Recent research in the area of using conic shaped fillets in the highly stressed regions of traditional force balances will be discussed, with preliminary numerical and experimental data results. A case study will be presented which discusses integration of this knowledge into a new high-capacity semi-span force balance.

Nomenclature

AF	Axial Force (lbs)
BMC	Balance Moment Center
CAD	Computer Aided Design
CPA	Critical Point Analyzer
DIC	Digital Image Correlation
DOE	Design of Experiments
EDM	Electrical Discharge Machining
FEA	Finite Element Analysis
FEM	Finite Element Model
FOS	Factor of Safety
FOV	Field of View
K_t	Stress Concentration Factor
MPC	Multipoint Constraint
NF	Normal Force (lbs)
NFMTC	National Force Measurement Technology Capability
PM	Pitching Moment (in-lbs)
RSM	Response Surface Methodology
RM	Rolling Moment (in-lbs)
SOF	Safety of Flight
YM	Yawing Moment (in-lbs)

I.   Introduction

In aeronautics ground testing applications, it is typically required that instrumentation be used to obtain high-precision measurements of aerodynamic loads on the test article of interest. Many applications use a

---

*Research Engineer. Aeronautics Systems Engineering Branch. NASA Langley Research Center.

†Aerospace Engineer. Structural and Thermal Systems Branch. NASA Langley Research Center.

force balance, which are multi-dimensional force transducers instrumented with strain gages used to measure components of aerodynamic load. Whether the instrument is an internal or external balance, load-cell based system or a dynamometer type instrument, the fundamental design concepts for how the loads are measured remain the same. These instruments are electro-mechanical devices that are designed to isolate the induced loads onto independent series of flexural elements, which act as structural springs.

Force balances are typically the single mechanical link between the test article and the model support system which is grounded to the facility, as shown in 1(a). As a result, it is essential that care be taken during the mechanical design of these instruments in order to ensure they meet specific stress requirements in order to ensure safety of the test facility.[1] Internal balances typically have two attachment points, referred to as the metric and non-metric ends, as shown in 1(b). In order to optimize the overall design of these instruments it is essential to look at both of the attachment points, as well as the flexural spring elements which are designed around the specific load requirements. The flexures on force balances are designed and strategically instrumented in such a manner that the response of the strain gage bridges are isolated from interactions due to other loadings. The flexure elements on most single-piece type balances are rectangular cantilever beam elements that bend under a design load. The bending of these elements is about the grounded end, which is directly coupled to the non-metric end of the balance. At the junction of the flexure to the bulkhead on both ends, there is typically a circular type radius that is machined in during fabrication, which represents a stress concentration.[2] This particular area is where the focus of this paper will concentrate on.

(a) Wind-Tunnel Model Aerodynamic Loads   (b) Internal Balance
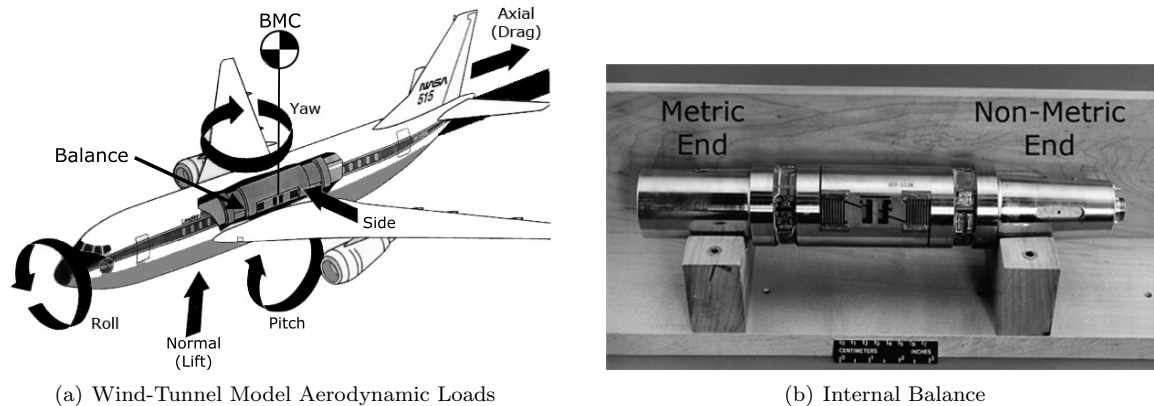
Figure 1. Standard Internal Balance Configuration in Wind-Tunnel Model

Current research within the aeronautics testing field defines measurement requirements that are becoming increasingly difficult to achieve with the current balance inventory available. Increases in the requirements on measurement precision and long-term confidence are beginning to drive the necessity for new design techniques for force balances. Due to the compact size and requirements on balance designs, there are often competing constraints and requirements where the benefits of traditional optimization techniques reveal their impact.

The current approach to balance designs within NASA typically target the design of the flexural regions of the structure based on the design load requirements, and the stress factor of safety (FOS) requirements established by the particular test facility. In the past, the design process typically involved performing hand calculations or developing spreadsheets that integrate all the necessary mechanics and beam equations to allow for computing the estimated stress state and measurement outputs from the design. Over the past few decades, the utilization of finite element analysis (FEA) packages have become more prevalent and have started to be integrated into the design process as an integral design tool. Current approaches still involve initial hand calculations to establish a baseline design, and then utilization of a FEA model to iterate towards a final design that satisfies all design requirements. While FEA has become more utilized in recent years, the use of it to optimize the overall design has not been explored to the fullest extent. The reason for this underutilization is partially due to the fact that most instruments have a relatively large number of design requirements (on the order of one to two dozen). Some of these requirements are considered and others are ignored based on engineering assumptions and principles. Another reason is the lack of understanding in how to use the available tools to perform this process.

II.   Motivation

Recent pushes in the aeronautics ground testing community are focused on real-time monitoring of the stress state of a balance.[3] Historically, the dominant focus during a wind-tunnel test to focus on the monitoring of balance signals and/or real-time computed forces and moments induced on the balance. These load monitoring techniques are aimed at ensuring the balance does not experience an overload condition that could potentially damage the balance or the test facility. Another recent approach within the community is to monitor the real-time stress state of the balance.[3,4] This process requires development of a refined FEA model that is used to explore the stress state of the balance during the initial design, in order to develop a set of stress coefficients that can be used to compute and monitor the balance real-time during use.

The requirement for a new semi-span balance to be used at the NASA Ames 11-Foot Transonic Wind-Tunnel was developed around 2010. As this new requirement was established, the facility approached the National Force Measurement Technology Capability (NFMTC).[5] A set of precisely defined design requirements were developed, including requirements on both the maximum allowable stress state and on the expected measurement output at a full-scale load for each of the five measurement components. The balance and reference axis system located at the balance moment center (BMC) for all aerodynamic forces and moments are shown in Figure 2. The specific requirements relating to the structural design of the instrument are given as:

- Force/Moment Design Loads:
    - NF = 30,000 lbs (along Y-axis at BMC)
    - AF = 3,000 lbs (along X-axis at BMC)
    - PM = 300,000 in-lbs (about Z-axis)
    - RM = 1,300,000 in-lbs (about X-axis)
    - YM = 150,000 in-lbs (about Y-axis)

- FOS > 3.0 on material ultimate strength for all hand calculations

- FOS > 2.0 on material ultimate strength for all FEA results

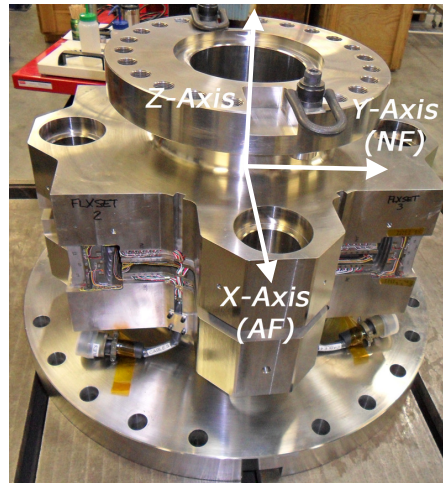- Full-scale output for all components > 1,400 micro-Volts at 1 Volt excitation

Figure 2. ARC-11-30K Reference Axis System

The primary objective was to develop an instrument utilizing non-traditional circular fillet radii at the base of the flexural elements, such that the localized stress concentrations within the balance could be reduced. The idea of minimizing localized stress regions on the flexure regions is somewhat counterintuitive, since the primary goal during most designs is to increase the stress as much as tolerable in order to achieve maximum output from the strain gages located in these regions. Thus as part of this effort, there exists the

challenge of balancing the design requirements with the requirement of integrating in new fillet geometry shapes, while still achieving the desired outputs from the strain gage bridges. A fillet is the Mechanical rounding of an exterior or interior corner or edge on any part design, with intent of creating a transition at this otherwise sharp junction in order to minimize the stress concentration.

With the integration of a new fillet geometry on the flexure regions, the goal is to reduce stress concentrations and as a direct result increase the fatigue life of the instrument. The fundamental design concept is to minimize localized stress concentrations on the instrument, where the locations of these stress concentrations are the regions where microscopic crack formation begins.[6] Basic fatigue theory indicates two phases of fatigue life: the *crack initiation period* and the *crack growth perod*. The stress concentration factor K_t is the critical parameter for prediction of crack initiation, therefore minimizing these localized values in the critically stressed areas of the balance is a critical step during design. During the *crack initiation period* the dominant phenomena driving the initiation are the surface effects (i.e., surface roughness, surface damage, surface treatments, soft layers). Once the *crack growth period* develops it becomes a bulk material phenomena, and surface effects no longer dominate. Proper care must be taken to ensure the surfaces of the critically stressed regions, to ensure the crack initiation process is not accelerated.

As part of the design and analysis, it was required that a set of stress coefficients be determined that are used to monitor the real-time stress state of the balance at the most critically stressed regions. The objective of this real-time monitoring is allow the facility to count fatigue life cycles over the complete time-history of the balance. Having this historical fatigue cycle counting ability allows the balance owner to schedule regular crack inspection intervals, and ultimately to determine when the balance needs to be pulled from service to avoid fatigue fracture. With the existing budget constraints and high visibility of ground testing facility operations, it has become increasingly important to ensure safety at the facilities by increasing the level of monitoring on the balance.

A. Load Monitoring Methods

During use of a balance in wind-tunnel testing operations, it is imperative that the user performs some form of balance signal monitoring . The wind-tunnel balance constitutes a Mechanically weak link in the transference of aerodynamic and inertial loads on the model to the support structure, and is the only structural link between the model and the support structure. In the event that the balance is damaged from an overload, it is feasible that the aerodynamic model being tested can break free and separate from the model support system, potentially causing significant damage to the test facility.

The reasons for monitoring the balance include, but are not limited to 1) minimizing risk of balance due to an overload condition either in model preparation outside of the tunnel, or overload inside of the test section during operation, 2) minimize risk to the wind tunnel facility due to a balance failure, 3) provide the user real-time feedback on the state of the balance/model during operation, and 4) monitor the real-time stress state of the balance which is used to compute fatigue cycles. For the purpose of this document, the type of physical hardware used to collect the data and the setup of the software/data acquisition will not be discussed. The only detail of importance is the general methodology, philosophies behind each method used, and general descriptions of how different facilities handle balance load monitoring during testing.

Across NASA facilities, many different balance monitoring techniques and methodologies are utilized, with varying degrees of fidelity and complexity. Some methods include: 1) monitoring only the strain gage bridge responses (units of milli-Volts or micro-Volts) and comparison of values against a full-scale output from the calibration, 2) computation of loads based on a simplified calibration matrix, 3) computation of balance loads based on the fully developed iterative calibration matrix, 4) monitoring of the stress-state of the balance for fatigue cycle counting purposes.

One option during test operations is to have the balance strain gage bridge signals connected to their respective signal conditioners and data acquisition system during testing, and to monitor the raw voltage (milli-volt, micro-volt) outputs of these channels. This method would compare the measured outputs during testing from each component to the full-scale output obtained during the balance calibration, and exceeding these outputs would signal an alarm during testing. This is the least preferred method, as only voltage signals are being monitored, and there is no way to correct for interaction terms that correct the signals for cross-talk. It is feasible that temperature drifts in the balance and analog circuitry and account for electrical signal shifts that are not corrected for, which could potentially lead to false confidence in the actual aerodynamic load or lead to occurrences where false alarms are triggered. An incremental improvement to measuring only voltage signals from the strain gage bridges is to apply the primary sensitivity to these signals in

order to monitor approximated engineering units. Generally speaking, load monitoring systems based on measurement of only voltages tend to be accurate to within approximately 5%.

The most common load monitoring technique is to monitor either the steady state static, or the steady state static and dynamic loads (aerodynamic forces/moments) imparted on the balance in the balance reference frame. The primary goal here is that the technique allows the user/operator to measure real-time loads in order to monitor whether the balance design load limits are exceeded, which could result in damaging of the balance or diminishing of data quality. Monitoring of the real time static/dynamic loads in engineering units is the next step in the evolution of load monitoring, as the voltage outputs from the individual strain gage bridges are passed through their respective calibration matrix in order to compute the nominal forces/moments. Typically for load monitoring, this would be the linear portion of the matrix that does not require load iterations for computational savings, but having the ability to correct for both linear and higher-order terms is advantageous to get the most precise estimate of real time aerodynamic loads. The form of the calibration matrix used for these real-time load computations varies based on facility, existing infrastructure and preference. Some facilities use a non-iterative matrix for these real-time computations, and some facilities use the iterative AIAA recommended 6x96 matrix.[7] The loads in engineering unit format can be filtered in order to decompose the signal into both static and dynamic components of load (filtering methodologies at this level vary). The interpretation of the total allowed load on the balance varies from facility to facility. Some facilities limit the balance based on total load (static plus dynamic, with no distinguishing between the percent contribution of each load type), and some facilities look at the filtered static and dynamic components and base their allowable limits off these ratios.

While most load monitoring methods track individual component loads, it is also advantageous to look at the total resultant load on the balance. One methodology used is known as the Critical Point Analyzer (CPA) method at the National Transonic Facility (NTF).[8] The CPA method utilizes estimated safe load limits based on the balance, model structure and support system stress analysis. The CPA method mixes different percentile components of the six balance components in order to arrive at a total safe load limit at any given location in the Mechanical chain, from the model support system through the balance and out to the aerodynamic model. Various percentile combinations can be invoked and monitored real-time. The CPA permits modifying safe load limits based on the situations where a model is being tested that is structurally weaker than the balance, and where the model support has a weaker load limit based on a mix of worst-case load vectors. The load limits are the vector sum of the force and moment components.

In recent years various wind tunnel facilities have started to develop methods for monitoring the real-time stress state of the balance during operation, for two purposes:

1. Develop a method for observing stress state in order to analyze how the balance is structurally being loaded relative to an established set of safe operating conditions. This is beneficial for simple monitoring purposes, and allows for real-time input on how the balance is behaving within the test matrix (potential for expanding test space, or input on where test space needs to be constrained to limit balance loads).

2. Perform fatigue life cycle counting of the balance over the balances life to determine when the balance either needs to be re-inspected for existence of cracks, or in order to determine when the balance meets the end of its fatigue life.

The rationale for discussing balance load monitoring is that the criticality of monitoring the balance during testing is directly coupled to the design of the instrument and the stress state observed during testing. Typically single-piece semi-span balances are designed to minimize their overall stiffness in each plane, in order to maximize the total measurement output from each strain gage bridge. As a direct result, the flexure beams are generally designed such that at their maximum design load the computed FOS approaches the acceptable limit by the facility. Therefore by design the instruments are as weak as possible, within acceptable limits. This inherent design philosophy requires that close monitoring of the balance be conducted during testing, in order to verify the balance and facility are operated in a safe manner at all times. The following sections will further highlight this.

III. Fillet Geometry Study

Recently, the realization that a necessary shift in the overall electro-Mechanical design methodology of force balance transducer within NASA resulted in the initiation of a study to look at fundamental design techniques, specifically geared at investigating the effects of fillet geometries on the balance stress state.

Common practice when designing and fabricating force balances is to utilize circular type fillet radii at the base of all flexure beams within the instrument, for the ease of machining and inspection. While these types of fillets are commonly used, they represent a localized area of stress concentration. Stress concentration theory, calculations and tables for various features and geometries are captured in great detail in the text.[9]

While circular fillet radii are commonly used in a many structural elements, particularly in force balance designs, it is well documented in the literature that non-constant variable radii geometries allow the designer to minimize localized stress concentrations.[10–13] Documentation suggests that with the correct selection of the geometry, based on the dominant loading condition (tensile/compressive vs. bending/torsion), stress concentration factors, K_t, can be reduced to a value of nearly unity. K_t is defined as

$$K_t = \frac{\sigma_{maximum}}{\sigma_{nominal}}$$

where $\sigma_{maximum}$ is the maximum localized stress located in the stress concentration, and $\sigma_{nominal}$ is the nominal stress in the member. A comparison of circular and variable radius fillet geometries are shown in Figure 3. Intuitively it can be seen that a variable radius allows for a smooth transition of the strain gradient across the curvature, as opposed to a circular radius which tends to focus the localized strain.
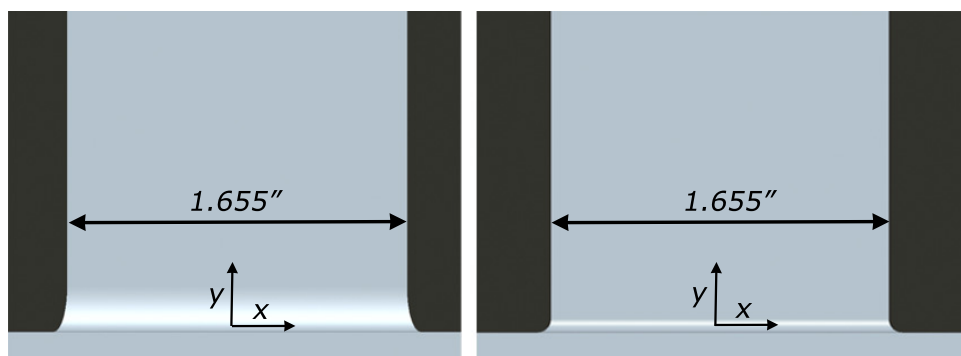

Figure 3. Left: Ellptical Fillet (x = 0.060", y = 0.200", rho = [($\sqrt{2}$)-1], Right: 0.060" Circular Fillet

Previous research by Baud in the 1930's/1940's led to significant data that suggests certain fillet profiles with non-constant geometry can lead to constant stress/strain across the fillets, where K_t approaches unity.[10, 11] The original postulation proposed by Baud was pulled from fluid mechanics, where an ideal frictionless fluid flow from the jet at the bottom of a tank could be mathematically described given the following equations:

$$x = 2\frac{d}{\pi}sin^2\frac{\theta}{2}$$

$$y = \frac{d}{\pi}\left[logtan(\frac{d}{\pi} + \frac{\pi}{4}) - sin\theta\right]$$

where x is the horizontal distance between the two asymptotes, y is the vertical distance between the the asymptotes, θ is the angle between the tangent to the curve and the x-axis, d is the total width of the fluid stream at the smallest width, and d_f is the total width at the exit of the jet.[9] It was noted from this original theory that the liquid at the boundary of the flow would have a constant velocity, therefore it was postulated that the same type of behavior may exist along the physical boundary of a fillet in a stressed member. Figure 4 provides a visual on the proposed concept along with the variables.[9]

Around the same time as Baud was developing his theory and experimenting with photo elastic test specimens, Thum and Bautz (1934) took the work of Baud and applied some corrections in accordance with the cube of the diameter.[14] This work resulted in a table of ratios that can be used to estimate the x and y dimensions of the fillet based on whether the dominant load case is tension/compression or bending/torsion. The table from Peterson's Stress Concentration Factor reference book (Table 3.1) is shown below in Table 1.[9] The importance of Table 1 will be shown in a later section, as the fillets selected for the the numerical/experimental study were derived from this.
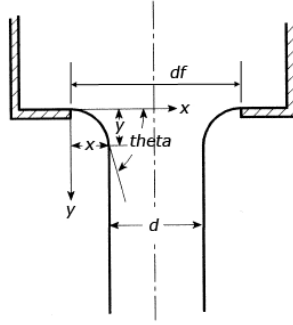
Figure 4. Ideal frictionless flow from opening in the bottom of a tank[9]

Table 1. Proportions for a Streamline Fillet[9]

y/d	d_f/d	d_f/d	y/d	d_f/d	d_f/d
0.00	1.636	1.475	0.30	1.187	1.052
0.002	1.610	1.420	0.40	1.134	1.035
0.005	1.594	1.377	0.50	1.096	1.026
0.01	1.572	1.336	0.60	1.070	1.021
0.02	1.537	1.287	0.70	1.051	1.018
0.04	1.483	1.230	0.80	1.037	1.015
0.06	1.440	1.193	0.90	1.027	1.012
0.08	1.405	1.166	1.00	1.019	1.010
0.10	1.374	1.145	1.30	1.007	1.005
0.15	1.310	1.107	1.60	1.004	1.003
0.20	1.260	1.082	∞	1.000	1.000

The streamline fillet proportions shown above identify x and y point coordinates that must be fit with a spline curve in order to define the curvature between the vertical and horizontal asymptotes. Depending on the available computer aided design (CAD) tools available, and ease of parametric modeling, one can either select a streamline proportion based on this data or a conical fillet geometry that closely approximates the streamline curve.

The majority of the published data in the field of non-circular fillets focuses on the case of two-dimensional geometry in a simple loading condition (tension, torsion or bending). For the case of the balance application the flexural elements of interest are three-dimension in nature, and the loading conditions observed during use can be quite complex. One of the complications with the three-dimension case is investigating how the stress field around the transition from one edge of the flexure to the other behaves, and how to measure the stress field in these areas. In the three-dimensional case where there exists four sides of a rectangular flexure beam the fillets from each edge must be merged at the intersection. This becomes more complex when the fillet geometries on each edge differ, requiring proper attention to ensure no additional stress concentrations are created due to machining imperfections.

A.   Finite Element Research

The design of the semi-span balance discussed previously revolved around the determination of an appropriate fillet geometry configuration that minimized stress concentrations and reduced the stress state of the balance at the maximum designed loading condition. Initial work in the area of determining the *optimal* fillet geometry focused on the pre-defined flexure geometry (heigh, width and thickness). Therefore this initial problem can not be defined as a true optimization problem in the sense of the definition, since many of the input variables were pre-defined and not adjustable. Therefore the focus of this research revolved around determining an appropriate set of fillet geometries that met a minimum set of requirements, with the primary requirement being that the total stress state in the flexure regions not exceed a level that would result in a FOS < 2.0.

The predominant CAD package used at NASA Langley to design and develop force balance instrumentation is the Pro/Engineer and Pro/Mechanica three-dimensional modeling and finite element analysis package. For the purpose of this study in order to simplify the design and increase the efficiency of design iterations, it was decided to approximate the streamline proportions with what is known as the *rho-factor* in Pro/Engineer. The rho-factor defines the segment of a conic arc, with varying conic shape, where the segment can take on the form of an ellipse, parabola or a hyperbola. The rho-factor can take a value from 0.05 to 0.95, where a perfect ellipse is equal to $[(\sqrt{2})-1]$, a parabola is equal to 0.5 and a hyperbola ranges from 0.5 to 0.95. A comparison in a later section of this paper will demonstrate the varying curvature based on a given set of rho-factors, and also makes a comparison between the varying rho-factor approximations and the streamline proportional curve based on the values in Table 1 above.

Figure 5 defines the dimensions of the conic arc PQ that represent the rho-factor. Line segments PR and QR are both tangent to the shown ellipse at points P and Q, respectively. Line segment RD intersects the line segment PQ at point D, where D is the midpoint of the line segment PQ. The rho-factor represents the ratio along a vector from the chord (PQ) through a point C to the vertex R. Point C is at the maximum distance CD, measured by a normal from the chord to the conic segment PQ.
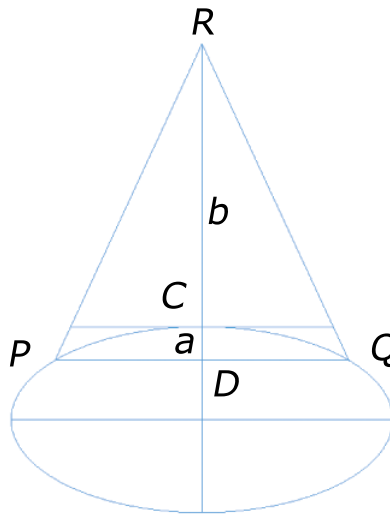

Figure 5. Rho-Factor Dimension of a Conic Arc

As mentioned above for this design the flexure research study revolved around a pre-determined flexure geometry. The nominal flexure geometries were allowed to be perturbed a small amount, but overall they were locked in based on the initial overall balance size and volume constraint requirements established by the customer. Also driving the flexure design as that this instrument was modeled after a pre-existing balance, but with higher design loads. The nominal flexure dimensions for the balance are given as height = 3.000 in, width = 1.655 in and thickness ranging from 0.200 in. to 0.227 in. Figure 6 defines the parameters of the test specimens designed for use as part of this study. The nominal flexure variables are shown, in addition to the fillet variables for both the long and short edges.

A formal numerical analysis experiment was designed utilizing design of experiment (DOE) and response surface methods (RSM), in order to run a preliminary FEA experiment to help provide information on appropriate fillet geometry that satisfied the requirements.[15, 16] For this study, a single flexural element was investigated under different loading conditions. The dimensions of this element match the nominal dimensions given above. The dependent and independent variables for this study are given below:

1. Dependent Factors:

    Maximum von Mises Stress (psi)

2. Independent Factors:

Long Edge Y-Dim. (low setting: 0.030 in., high setting: 0.300 in.)

Long Edge X-Dim. (low setting: 0.030 in., high setting: 0.300 in.)

Short Edge Y-Dim. (low setting: 0.030 in., high setting: 0.300 in.)

Short Edge X-Dim. (low setting: 0.030 in., high setting: 0.300 in.)

Long Edge Rho-Factor (low setting: 0.10, high setting: 0.80)

Short Edge Rho-Factor (low setting: 0.10, high setting: 0.80)

3. Test Conditions:

Tensile Loadings (12,000 lb maximum)

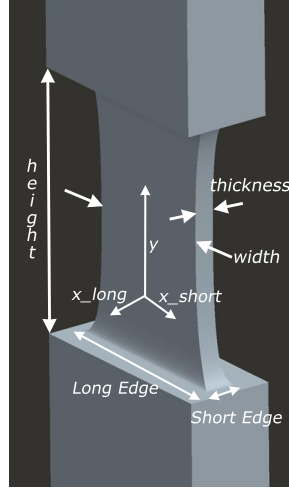Torsion Loadings (1,250 in-lb maximum about the flexure centerline axis)

Figure 6. Test Specimen - Edge Variable/Parameter Definition

As stated above the primary output response of interest is the maximum von Mises stress computed along the fillet geometry. The maximum von Mises stress is computed and output from the FEA. The von Mises stress is competed as:

$$\sigma_{vonMises} = \sqrt{\frac{(\sigma_1 - \sigma_2)^2 + (\sigma_2 - \sigma_3)^2 + (\sigma_1 - \sigma_3)^2}{2}}$$

where $\sigma_{vonMises}$ is the computed von Mises stress from the principal stresses (σ_1, σ_2, σ_3) at each point in each axis.[17]

Based on the above independent variables a set of eight specimens were analyzed via FEA, and the data was exported to allow for 3D visualization of the localized stress and strain profiles in the fillet regions. The specimens analyzed are shown in Table 2. In order to minimize the total number of fabricated specimens and performed experiments, each specimen was modeled to have a different fillet geometry on each end of the flexure. Specimen number 8 will be referenced in a later section, as this is the specimen that contains the final selected geometry that was integrated into the final balance design.

B. Experimental Research

The primary objective of this fillet study research was to conduct numerical analysis of varying fillet geometries to demonstrate the concept of the improvements provided by non-circular fillets and to validate these results through physical experimentation. The difficulty with validating the FEA results was the determination of an appropriate measurement system capable of the required precision of stress/strain measurements during experimental testing. The results from FEA provide global three-dimensional contour plots of the stress and strain field distributions along the specimen under a given loading. The FEA is capable of providing point measurements of stress and strain, if the model is properly configured.

Table 2. Fillet Geometry Specimens for 30K Balance Design

Specimen	Long Edge			Short Edge		
	X-Dim.	Y-Dim.	Rho Factor	X-Dim.	Y-Dim.	Rho Factor
1a	0.060	0.060	circular	0.060	0.060	circular
1b	0.060	0.250	0.414	0.060	0.250	0.414
2a	0.100	0.250	0.414	0.060	0.1 00	0.550
2b	0.060	0.140	0.550	0.120	0.140	0.414
3a	0.090	0.250	0.414	0.075	0.140	0.550
3b	0.060	0.140	0.550	0.030	0.140	0.550
4a	0.060	0.140	0.550	0.075	0.140	0.414
4b	0.060	0.250	0.800	0.030	0.600	0.800
5a	0.060	0.060	0.414	0.075	0.300	0.300
5b	0.120	0.250	0.600	0.060	0.250	0.300
6a	0.120	0.250	0.300	0.100	0.060	0.600
6b	0.060	0.250	0.550	0.075	0.060	0.414
7a	0.090	0.200	0.414	0.060	0.140	0.800
7b	0.100	0.200	0.800	0.100	0.100	0.300
8a	0.072	0.363	0.500	0.276	1.390	0.500
8b	0.072	0.363	0.500	0.276	1.390	0.500
9a	0.060	0.060	circular	0.060	0.060	circular
9b	0.030	0.030	circular	0.030	0.030	circular

The specimens identified in Table 2 above were fabricated for experimental validation testing, with the objective of comparing the results against the numerical FEA results. Each specimen was fabricated using conventional die-sink electrical discharge machining (EDM) techniques, the the fillet geometries are *burned* into the part, rather than using conventional machine tools or die fabrication processes. Upon completion of each specimen, the fillet geometries along all curvatures were inspected using an optical comparator to compare the as-built shape of each fillet to the nominal design shape to determine the variation. Approximating the variance of the final as-built geometries provided the opportunity for comparison against the nominal, in order to perform a sensitivity study using FEA.

For the purpose of this study, it was determined that two different measurement techniques would be employed during experimental testing. The two methods used were instrumentation of the specimens with conventional foil strain gages, and use of a digital visual correlation system (DIC) system. The conventional foil strain gages allow for measuring discrete *point* measurements of localized strain, and the DIC system provides the capability of measuring either two- or three-dimensional stress and strain contours over the field of view (FOV) of interest.
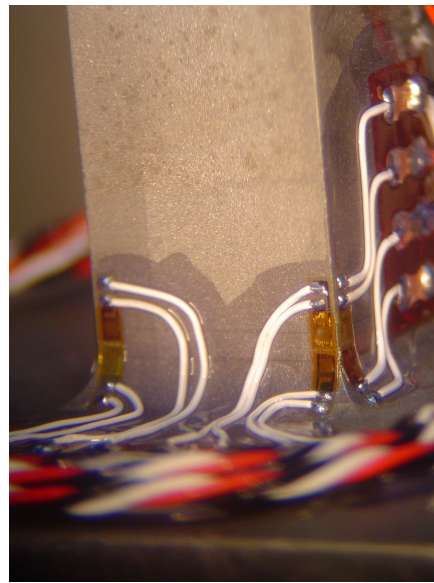
Figure 7 provides two images which show opposite ends of specimen 1, with the foil strain gages located along the circular and non-circular fillets. The strain gages used along the fillet radii were Micro-Measurements uni-axial J3K-06-S1394-350 transducer quality gages, with nominal trimmed dimensions of 0.030 in. x 0.078 in. The FEA model was setup to provide point estimates of stress and strain at the center of the measurement grids as located along the curvature of the fillets. Also shown in the figure are a strain gage located away from the fillet - this sensor was used to measure the $\sigma_{nominal}$ to calculate the K_t. Another foil strain gage was located at the center mid-plane of each flexure, in order to capture a more accurate measurement $\sigma_{nominal}$ away from the fillet.

The DIC system used for initial testing was provided by Correlated Solutions, Inc., and is shown in Figure 8. This system allows for three-dimensional measurements, where two sets of cameras are used (each set containing two cameras). The basic theory which the DIC system is built around use of photogrammetric techniques to collect digitized images that are used to computed in-plane and out-of-plane measurements of displacement.[18] Through the process of calibrating the systems and algorithms, the measured displacements from the digitized images are used to compute other engineering parameters (strain and stress). The displacement measurements are achieved by placing a type of grating or speckle pattern on the test specimen, where the collected images from the camera system are used to measure the relative change in the location of the speckle pattern *targets* from successive views collected during testing.

Figure 8 shows one of the setups used during initial testing. Shown in this figure is the test specimen in the center of the tensile testing machine, and the two sets of DIC cameras setup to ensure the entire fillet

(a) Gage Placement along Non-Circular Fillet   (b) Gage Placement along Circular Fillet

Figure 7. Specimen 1 Foil Strain Gage Placement (Circular and Non-Circular Fillets)
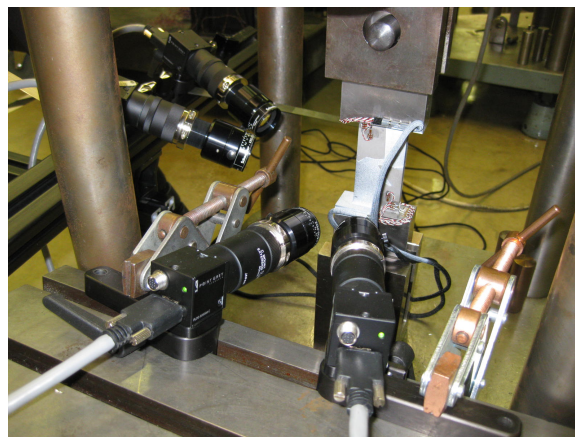

Figure 8. Fillet Study Specimen Testing in Tension Machine

of interest is in the FOV. Two of the difficulties that arose during testing were the difficulty of applying the appropriate speckle patter size to enable an appropriate level of measurement resolution, and the ability to focus the cameras on the small FOV of interest in order to capture the small three-dimensional fillet shapes. The challenge with applying the correct speckle pattern and particle size to the area of interest was the identification of a particle type and application method, in order to ensure small enough particle size to increase the measurement resolution while establishing a repeatable application process. The final methodology used for the test specimens involved the use of toner particles used in commercial printer cartridges, and applying them to a white base coating via an air canister.

Setup of the camera system presented some challenges. With the FOV being so small relative to typical test specimens, the available volume around the specimen requires unique setup procedures. The objective was to measure three-dimensional strain contours, which requires a total of four cameras as shown in Figure 8, with two cameras per system. The cameras are setup as shown in Figure 10. This test configuration required close attention to detail to ensure the cameras were properly focused on the test specimen fillet area of interest, and to ensure they were setup to capture the correct FOV spanning around the intersection of the fillets from the two sides of the flexure. The straight black marks shown in Figure 8 indicate the transition from the flat into the curved portion of the fillet along each side of the flexure beam. These marks were
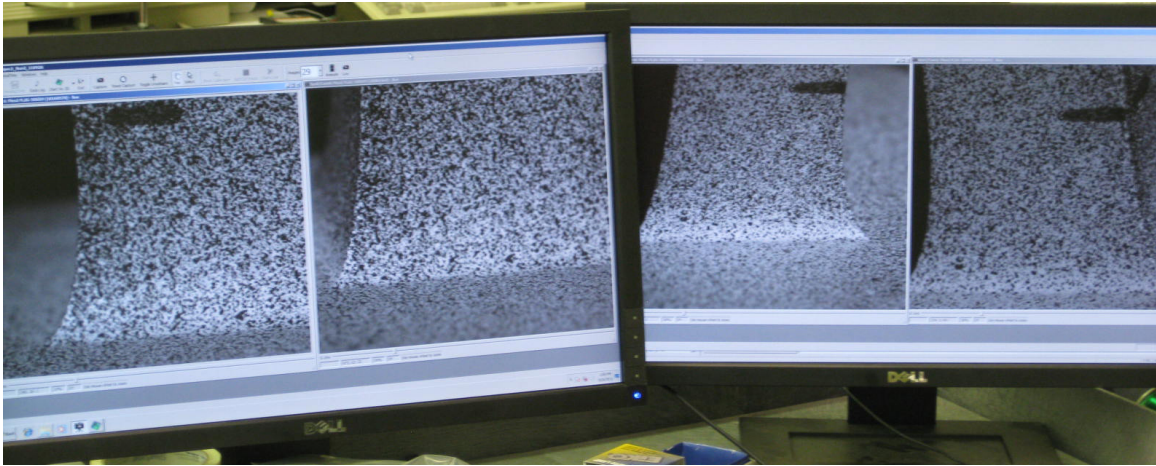
Figure 9. DIC Images of Specimen 1 Fillet Intersection (Both Camera Sets)

critical in setting up the cameras, to ensure the entire fillet region was in the FOV. The calibration process, not discussed in this paper, is integral to the measurement system setup, as this establishes the level of accuracy and precision obtained during all measurement data collected from the system. The measurement resolution in the data collected from the DIC system is dependent on the calibration process. The nominal measurement resolution estimated during each experiment was approximately +/- 50 μ-strain.
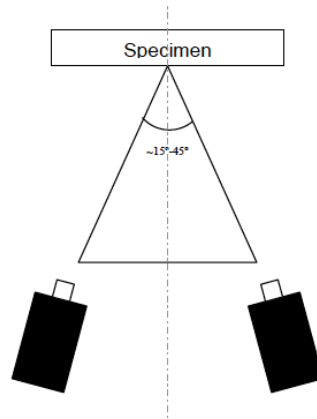

Figure 10. DIC Two-Dimensional Camera Setup Configuration

Table 3 reveals the results from the FEA test cases, and the experimental validation cases. Shown in this table are the measured results during the experimental cases from both the discrete strain gages located along the fillet curvature, as well as the results measured from the DIC system. It should be highlighted that the FEA and DIC results compare very well with each other, typically within 5%, but the strain gage data typically varies anywhere from 5-40%. This discrepancy is due to the fact that the strain gages are discrete point measurements, and the strain in the region of the measurement grid is averaged. Therefore in the presence of a high strain-gradient, it is likely that the averaging over the grid area is resulting in an un-prediction of the true strain. Some of the variation between the discrete and global measurements can also be attributed to the mis-alignment of the strain gages in these regions, as well as non-ideal bonding of the gages. Installation of strain gages in these tight regions of extreme curvature is difficult and can lead to potential inaccuracies in the measured data. Initial testing primarily focused on tensile experiments, since it was determined from the initial analysis of the ARC-11-30K balance that the tensile load was the pre-dominant load on the flexures.

An interesting observation during both the FEA and experimental testing is that for all the specimens, with the exception of specimen 8, the peak strain and stress always occurs at the base of the flexure where

the two edge fillets intersect. For specimen 8 the peak stress/strain occur near the mid-plane away from the fillets, which implies the fillet geometry is behaving appropriately and the nominal K_t value is approaching unity. Specimen 6 was permanently damaged during installation into the tensile testing machine, therefore no data was collected. Specimen 9 was built after the final geometry was selected for the ARC-11-30K balance, and has not yet been tested.

<div align="center">

Table 3. FEA versus Experimental Results Comparison for Test Specimens

</div>

			TENSION				TORSION	
			Experiment	Experiment			Experiment	Experiment
	FEA	FEA	Strain Gage	DIC System	FEA	FEA	Strain Gage	DIC System
Specimen	(ksi)	(μ-strain)	(μ-strain)	(μ-strain)	(ksi)	(μ-strain)	(μ-strain)	(μ-strain)
1a	72.40	2,784	2,550	2,710	102.80	3,953	not tested	not tested
1b	45.70	1,770	1,290	1,810	60.67	2,201	not tested	not tested
2a	48.07	1,822	1,335	1,785	67.82	2,407	not tested	not tested
2b	56.92	2,073	1,825	1,994	78.50	2665	not tested	not tested
3a	49.11	1,721	1,580	1,739	74.38	2,663	not tested	not tested
3b	67.14	2,568	1,660	2,499	84.58	3,005	not tested	not tested
4a	51.83	1,833	1,765	1,811	125.71	4,641	not tested	not tested
4b	83.19	3,232	2,390	3,097	180.40	6,545	not tested	not tested
5a	56.27	2,038	1,290	2,114	78.79	2,878	not tested	not tested
5b	60.38	2,255	2,050	2,241	60.60	2,265	not tested	not tested
6a	40.43	1,583	damaged	damaged	59.67	2,138.	damaged	damaged
6b	76.14	2,761	damaged	damaged	98.35	3,408.	damaged	damaged
7a	74.21	2,881	2,370	2,793	93.60	3,546	not tested**	not tested**
7b	62.51	2,293	1,400	2,216	71.32	2,586	not tested**	not tested**
8*	**35.99**	**1,323**	**1,297**	**1,311**	**79.83**	**2,294**	**not tested****	**not tested****
9a	64.21	2,429	not tested	not tested	87.56	3403	not tested**	not tested**
9b	141.40	5,094	not tested	not tested	161.80	5811	not tested**	not tested**

*Specimen 8 has same fillet geometry on both ends of flexure. **Not Tested = tests have not yet occurred, but are planned.

An example of one of the images produced from the measurement data processed by the DIC system is shown in Figure 11 below. This strain contour plot is from a single set of cameras during testing. The view from the opposite side of the fillet is not shown. Figure 11 clearly shows some voids in the contour along the curvature - these are results of highly distributed speckle targets, where the system is not able to extract any information in that area. This figure reveals the region along the perimeter of the fillet radius is the location of the maximum strain, and increases to a maximum at the intersection of the two edge fillets. For reference the peak strain at the edge fillet intersection for this experiment was measured with the DIC system to be 2,710 μ-strain.
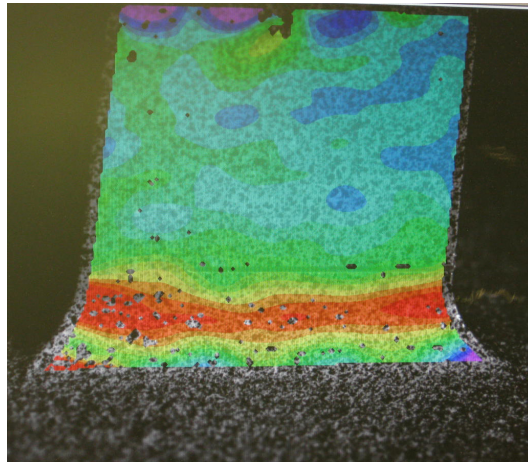

Figure 11. Strain Contour Example from DIC System (Specimen 1 - Circular Fillet); Legend not shown, Maximum red intensity represents peak strain of 2,800 μ-strain.

IV. ARC-11-30K Balance Design

A. Pro/Mechanica Finite Element Analysis

Pro/Mechanica was used during the initial balance design and development to analyze the stress state of the balance under the influence of the design loads. At the onset of the design, the initial design incorporated convention circular radii, as there was no stringent requirement on use of non-circular fillets. The design was iterated until a design was achieved that met the stress requirements, but the FOS achieved were on the borderline of the acceptable value. During the initial preliminary design review, the review board recommended looking at non-circular radii in order to decrease the stress state while strain maintaining the require levels of measurement output. After completing the work discussed in the above sections relating to the fillet study optimization for this balance design, a final design was achieved that yielded a FOS > 2.0 and met all other requirements. The material properties used for the analysis are shown in Table 4.

Table 4. Balance Material Properties

Alloy	15-5 PH S.S. H900
Modulus of Elasticity	28,500,000 psi
Modulus of Rigidity	11,200,000 psi
Ultimate Tensile Strength	190,000 psi
Yield Tensile Strength	170,000 psi
Density	0.285 lb/in^3

The fillets used for this balance are based on the thickness and width of the final flexure dimensions. The flexure dimensions were designed in an iterative nature to size them appropriately to yield the required measurement outputs and estimated maximum web stress values. The final flexure width for all flexures was designed to be 1.655 in., and the final flexure thickness was chosen to be 0.227 in. [beams 1 thru 6] and 0.200 in. [beams 7 and 8]. For these flexure dimensions, the resulting fillet heights/lengths were computed for both tension and torsion loading proportions. In order to determine whether the tension/torsion loading proportion dimensions were appropriate for this balance design, several FEA cases were run on the final balance design with the 2 sets of fillet geometries. It was found that the tension streamline fillet dimensions yielded the minimal maximum von Mises stress values, so the final balance design uses tension proportion dimensions.

The streamline coordinates define a unique curve that minimizes the resulting K_t values. Within Pro/Engineer, the standard radius/fillet generation feature allows for either circular or conic type fillet curvatures. Instead of inserting the streamline spline curve points into Pro/Engineer in order to generate solid geometries for the fillets, it was decided to approximate the streamline fillet with a conic fillet. This decision was made for ease of modeling, and to decrease the time associated with changing the fillet dimensions/geometry during iterations of different designs during the design process.

Figures 12 and 13 plot out the streamline fillet geometry for the final flexure width dimension of 1.655 in., for both the tensions and torsion loading conditions. In addition to the streamline fillet geometry curvature, varying conic fillets with varying rho values (rho values define the conical nature of the curve in between the start/end points generated from the streamline values) were plotted to determine which conic geometry closely approximated the streamline geometry. For the case where tensions loadings are the dominant load case, a rho value of approximately 0.500 closely approximates the streamline curve (see Figure 12). For the case where torsion/bending loadings are the dominant load case, a rho value of approximately 0.700 closely approximates the streamline curve (see Figure 13). For the final balance design, the final fillet dimensions for the primary flexures (excluding the axial force stress riser) use the tension loading proportion dimensions (height/length/rho-factor).

The localized stress contour plots in the flexure region for the original design (circular fillets) and the final design (conical approximated streamline fillets) are shown in Figure 14. It can be seen that the circular fillet results in a more localized concentration of the stress at the base of the flexure, while the conical fillet more smoothly distributes the load and stress over the entire transition of the fillet curve. The maximum von Mises stress for the baseline design using circular fillets was approximately 125 ksi, while the final design utilizing conic fillets resulted in a maximum value of 95 ksi. This reduction in stress is a direct result of the new optimized fillet geometry for this balance design.

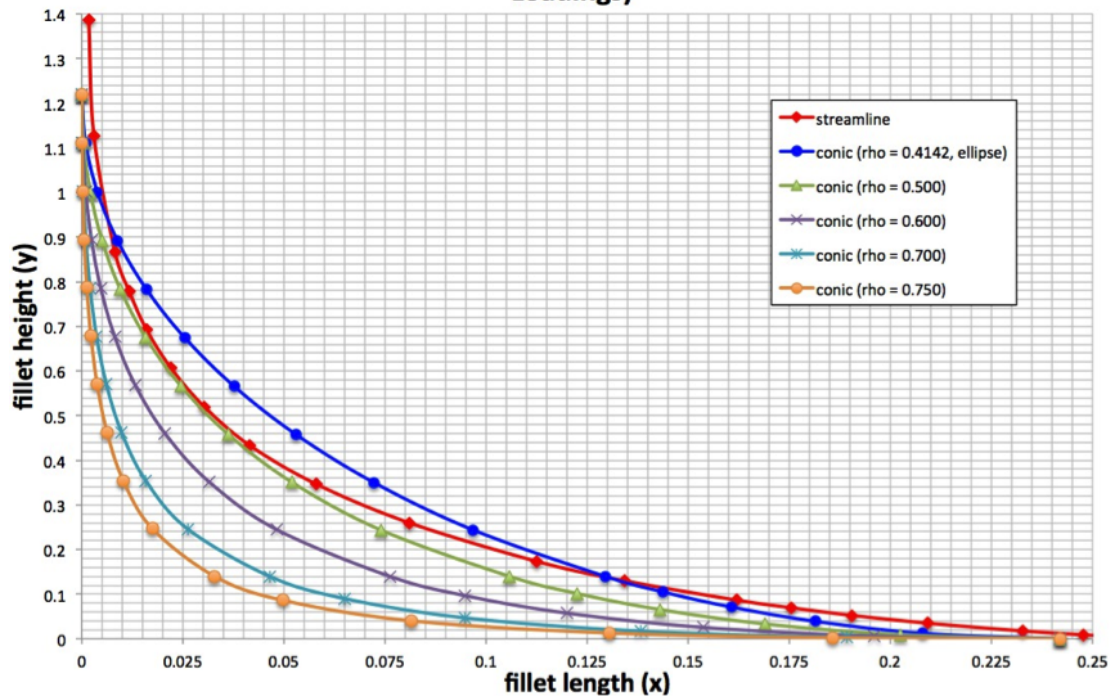**Comparison of Streamlined Fillet vs. Various Conic Fillets (Tension Loadings)**

Figure 12. Streamline vs. Conic Fillet Comparison (tension proportions)

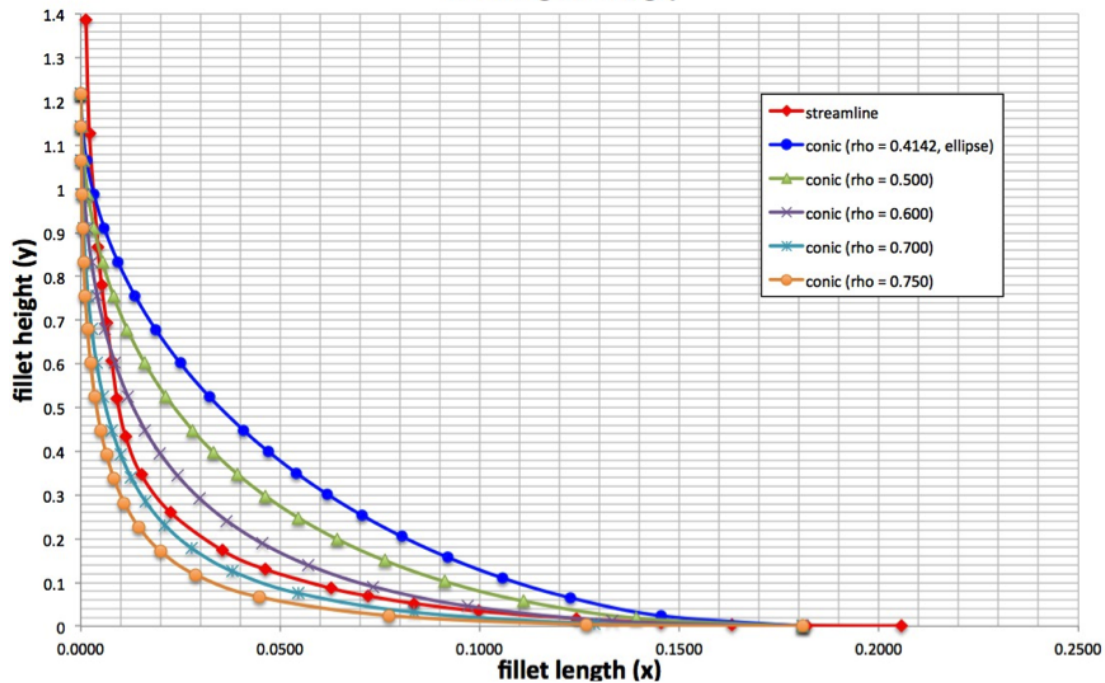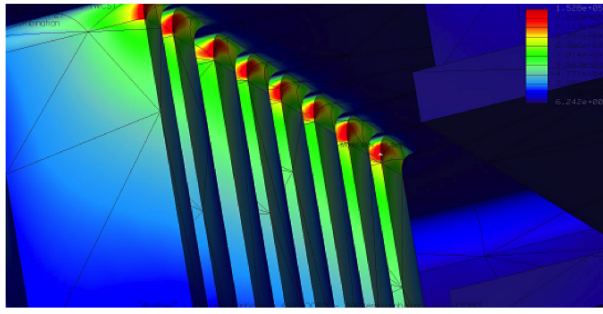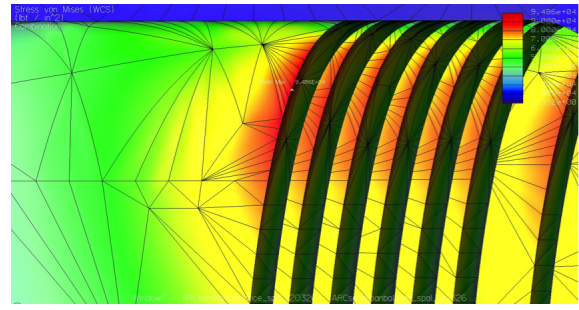**Comparison of Streamlined Fillet vs. Various Conic Fillets (Torsion/ Bending Loadings)**

Figure 13. Streamline vs. Conic Fillet Comparison (torsion/bending proportions)

9th International Symposium on Strain-Gage Balances

(a) Baseline Design (circular fillets)

(b) Final Design (conical fillets)

Figure 14. Localized Stress Concentration Comparison for Baseline and Final Balance Flexure Geometry Designs

Table 5. Pro/Mechanica FEA Load Cases and Results

Load Case	NF (lb)	AF (lb)	PM (in-lb)	RM (in-lb)	YM (in-lb)	Maximum von Mises Stress (ksi)	Maximum Principal Stress (ksi)	FOS (ultimate)
1	+30000	0	0	0	0	20.45	20.50	9.29
2	0	+3000	0	0	0	20.38	20.36	9.32
3	0	0	+30000	0	0	59.01	61.66	3.22
4	0	0	0	+1300000	0	54.76	62.94	3.47
5	0	0	0	0	+150000	7.58	7.76	25.04
6	+30000	+3000	+300000	+1300000	+150000	92.31	70.78	2.06
7	+30000	-3000	+300000	+1300000	+150000	86.46	88.20	2.20
8	-30000	-3000	+300000	+1300000	+150000	93.02	94.65	2.04
9	-30000	+3000	+300000	+1300000	+150000	85.02	80.80	2.23
10	+30000	-3000	-300000	+1300000	+150000	83.72	85.26	2.27
11	-30000	-3000	-300000	+1300000	+150000	92.73	72.86	2.05
12	**+30000**	**+3000**	**-300000**	**+1300000**	**+150000**	**94.86**	**97.49**	**2.00**
13	-30000	+3000	-300000	+1300000	+150000	85.86	88.85	2.21

B.   MSC Nastran Linear Static and Modal Analyses

A finite-element model (FEM) of the ARC-11-30K semi-span force balance was created in MSC Patran v2012 using the imported Pro/Engineer three-dimensional solid CAD geometry. Linear static and modal analyses of the balance FEM were then performed using MSC Nastran v2012. The rationale for using MSC Patran to perform an additional analysis of the ARC-11-30K balance design was two-fold: 1) verify results from analysis using Pro/Mechanica, 2) MSC Nastran has the ability to output nodal data for all finite element nodes which is required in order to perform the critical stress node analysis.

1.   Mesh Convergence Study

The critical areas of the balance are the flexure regions and the transition regions from the flanges to the metric and non-metric bulkhead sections. To obtain accurate stresses and strains in these areas, the balance FEM must be properly meshed. Mesh convergence studies were performed by generating increasingly refined balance FEMs, performing linear static analyses of these FEMs, and then reviewing the displacement and von Mises stress results in the critical areas. The mesh was considered appropriately refined when the displacement and von Mises stresses did not change significantly in models of further mesh refinement.

Increasingly refined FEMs of the balance were generated by varying the global edge length and mesh refinement options such as the maximum element height per length and the minimum edge length per global edge length. The global edge length was varied from 1.25 to 0.35 inches. The maximum element height per length was varied from 0.1 (default) to 0.025, and the minimum edge length divided by global edge length varied from 0.2 (default) to 0.1. A linear static analysis of each FEM was performed using MSC Nastran, and the resulting displacement and von Mises stress results in the flexures and the flange-to-bulkhead transition regions reviewed. The peak von Mises stresses in the flexures and the flange-to-bulkhead transition regions

for each mesh configuration analyzed are listed in Table 6.

Both the global edge length and maximum element height per length had a large effect on the magnitude of the von Mises stresses in the flexures. There was less than a 3.6% change in peak flexure von Mises stress for global edge lengths of 0.75 and less and maximum element height per lengths less than 0.05. The magnitude of von Mises stress in the flange-to-bulkhead transition regions were more affected by the maximum element height per length and minimum edge length per global edge length. There was less than a 5.9% change in peak von Mises stresses in the flange-to-bulkhead transition regions for maximum element height per length values of 0.05 or less and minimum edge length per global edge length of 0.1. Given the amount of curvature in the balance geometry, a global edge length of 0.5, a maximum element height per length of 0.025, and a minimum edge length per global edge length of 0.1 provided the greatest degree of mesh refinement in the flexures and flange-to-bulkhead transition regions. Further refinement of these mesh parameters produced models too large for meshing and results post-processing.

Table 6. MSC Nastran Mesh Convergence Results

Global Edge Length (in.)	Maximum Element Height Per Length	Minimum Edge Length per Global Edge Length	Peak Flexure Stress (ksi)	Peak Top Flange to Balance Block Transition Region Stress (ksi)	Peak Bottom Flange to Balance Block Transition Region Stress (ksi)
1.25	0.0375	0.10	95.02	70.35	33.51
1.00	0.100	0.20	91.14	63.48	31.43
1.00	0.050	0.10	96.24	70.05	33.42
1.00	0.050	0.20	96.54	69.56	33.79
1.00	0.025	0.10	95.60	71.21	33.96
0.80	0.025	0.10	95.55	69.70	33.98
0.75	0.100	0.20	93.12	62.81	31.86
0.50	0.100	0.20	94.67	61.45	33.04
0.50	0.050	0.10	96.39	67.25	33.94
0.50	0.025	0.10	93.23	69.57	33.87
0.35	0.025	0.10	93.10	69.74	33.87

2. Finite Element Model (FEM)

The FEM used for linear static analyses consisted of approximately 2.6 million 10-node tetrahedral elements, 3.9 million nodes and 11.6 million degrees-of-freedom. This model, shown in Figure 15, was generated using the material properties of 15-5 PH stainless steel in Table 4 and the following mesh parameters as determined from the mesh convergence study: global edge length of 0.5, maximum element height per length of 0.025 and minimum edge length per global edge length of 0.1. A much coarser FEM was used for the modal analysis. This model consisted of approximately 500,000 10-node tetrahedral elements, 750,000 nodes and 4.5 million degrees-of-freedom. The modal FEM was generated using a 0.5 global edge length as was used for linear static FEM, and the default maximum element height per length and minimum edge length per global edge length values of 0.1 and 0.2, respectively.

The ARC-11-30K semi-span balance design loads (sign convention for a left wing model) were listed above in a previous section of this paper. The ARC-11-30K semi-span balance was analyzed for the six load cases shown in Table 7. Load cases 1 thru 5 corresponded to the individual design loads given above. Load case 6 consisted of a combination of all five design loads.

For each load case, the forces and/or moments were applied relative to the balance coordinate system to a node located at the BMC. A multipoint constraint (MPC) element was used to transfer the load generated by the forces and moments resolved about the BMC to the top surface of the metric flange of the balance. The applied loads are shown on the ARC-11-30K FEM in Figure 16. The orientation about each axis for each balance design force and moment was described in the Motivation section of this paper.

The balance was constrained on the non-metric flange by fixing all 3 translational and 3 rotational degrees-of-freedom at each node on the interior of each flange mounting hole as shown in Figure 16.
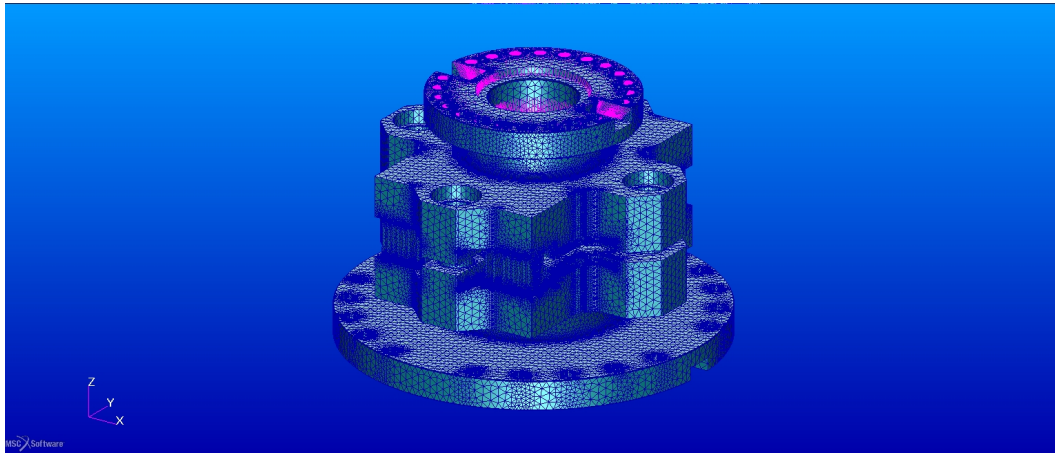
Figure 15. ARC-11-30K Semi-Span Balance MSC Patran Finite-Element Model

Table 7. ARC-11-30K Semi-Span Balance Load Cases

Load Case	NF (lb)	AF (lb)	PM (in-lb)	RM (in-lb)	YM (in-lb)
1	30,000	0	0	0	0
2	0	3,000	0	0	0
3	0	0	300,000	0	0
4	0	0	0	1,300,000	0
5	0	0	0	0	150,000
6	30,000	3,000	300,000	1,300,000	150,000
7	30,000	-3,000	300,000	1,300,000	150,000
8	-30,000	-3,000	300,000	1,300,000	150,000
9	-30,000	3,000	300,000	1,300,000	150,000
10	30,000	-3,000	-300,000	1,300,000	150,000
11	-30,000	-3,000	-300,000	1,300,000	150,000
12	30,000	3,000	-300,000	1,300,000	150,000
13	-30,000	3,000	-300,000	1,300,000	150,000

3. Analysis and Results

A modal analysis of the ARC-11-30K semi-span balance, subject to the boundary conditions above, was performed using MSC Nastran. The MSC Nastran modal results were then compared to the modal analysis results computed from Pro/Mechanica. The modal analysis results determined from Pro/Mechanica and MSC Nastran compared well as shown in Table 8.

Table 8. ARC-11-30K Semi-Span Balance Modal Analysis Results Comparison

Mode	Mode Shape	Frequency (Hz) Mechanica	Frequency (Hz) MSC Nastran	% Difference
1	AF Translation	129.2	128.1	0.9%
2	RM Rotation	302.5	300.2	0.8%
3	PM Rotation	350.4	348.5	0.5%
4	SF Translation	465.2	460.8	0.9%
5	AF Translation + YM Rotation	507.2	503.3	0.8%
6	NF Translation + RM Rotation	928.0	922.7	0.6%

Linear static analyses of the ARC-11-30K semi-span balance FEM, subject to the applied loads and boundary conditions above, were performed using MSC Nastran v2012. The results from the MSC Nastran linear static analyses were reviewed and then compared to the linear static Pro/Mechanica analysis results. Of particular interest were the maximum von Mises and Maximum Principal stresses listed in Table and 9. For all load cases, the MSC Nastran von Mises and Maximum Principal stresses in the flexures compared
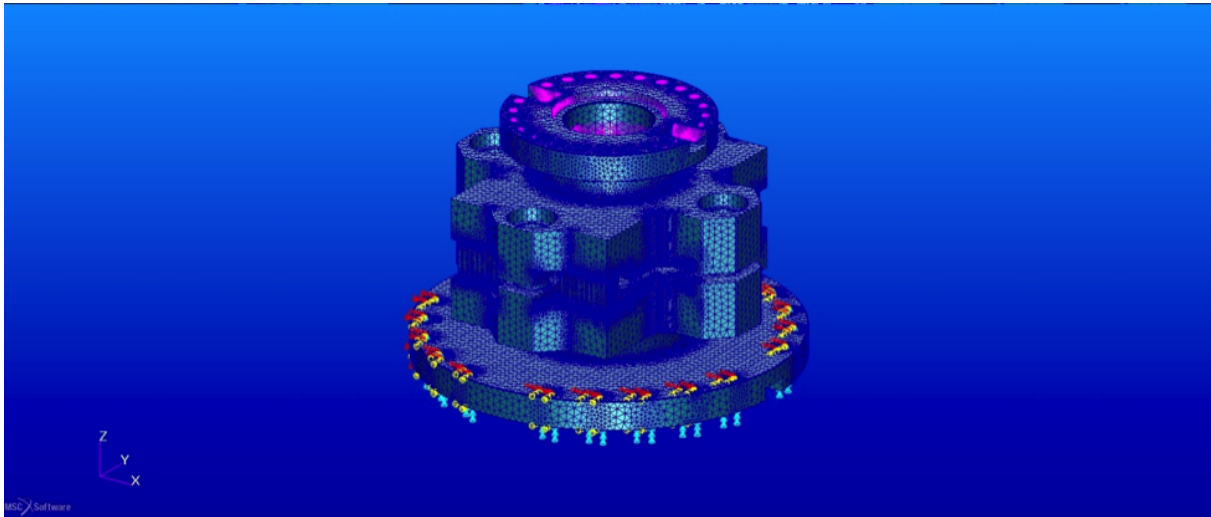
Figure 16. ARC-11-30K Balance FEM Applied Loads and Boundary Conditions

within 6% of the Pro/Mechanica von Mises and Maximum Principal stress. This error band was considered reasonable given that it was challenging coming up with a mesh density in MSC Patran that matched the fidelity of mesh in the Pro/Mechanica model without producing FEMs too large for meshing and results post-processing. The MSC Nastran von Mises and Maximum Principal stresses in the flange-to-bulkhead transition regions were within 10 to 13% of the Pro/Mechanica von Mises and Maximum Principal stresses. Given that MSC Patran allowed for significant refinement in these regions, the flange-to-bulkhead transition regions stresses determined using MSC Nastran are likely more accurate.

Table 9. ARC-11-30K FEA Comparison - Maximum von Mises and Principal Stress

Load Case	Max. von Mises Stress Stress (ksi)		% Error in Max. von Mises Stress	Max. Principal Stress Stress (ksi)		% Error in Max. Principal Stress
	MSC Nastran	Mechanica		MSC Nastran	Mechanica	
1	19.80	20.45	-3.21	20.32	20.50	0.86
2	19.17	20.38	-5.96	19.55	20.36	3.97
3	56.68	59.01	-3.93	58.80	61.66	4.63
4	59.91	54.75	9.42	68.86	62.94	-9.41
5	7.33	7.58	-3.28	7.52	7.75	3.02
6	93.23	92.31	1.00	80.07	70.78	-13.13
7	83.10	86.46	-3.88	83.98	88.20	4.78
8	93.07	93.02	0.06	93.97	94.65	0.72
9	85.03	85.02	0.01	83.68	80.80	-3.57
10	83.66	83.72	-0.07	83.66	85.26	1.88
11	92.90	92.73	0.19	71.25	72.86	2.21
12	**93.62**	**94.86**	**-1.30**	**94.32**	**97.49**	**3.24**
13	82.52	85.86	-3.89	86.11	88.85	3.08

The highlighted load case is the worst-case from the original design analysis

The von Mises stresses in the balance for Load Case 1 in the flexure region are shown in Figure 17(a), where the maximum von Mises stress for this design load is 19.80 ksi. The von Mises stresses in the balance for Load Case 2 in the flexure region are shown in Figure 17(b), where the maximum von Mises stress for this design load is 19.17 ksi.

C. Critical Nodal Stress Analysis

For each load case analyzed, the information provided in Table 10 for each node in the model was exported to a MSC Patran results text (.txt) document. The MSC Patran results text documents are imported into
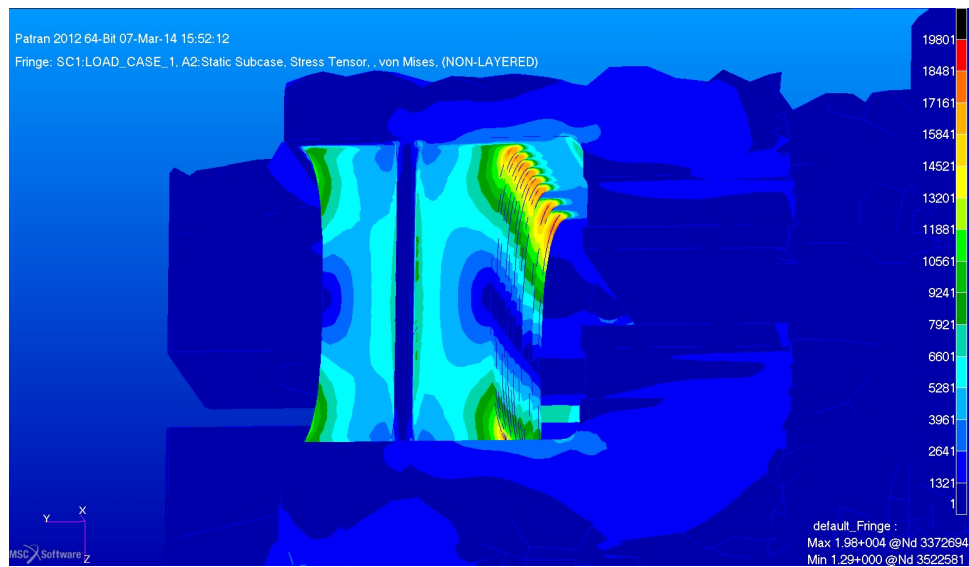
(a) ARC-11-30K Flexure Max. von Mises Stress within Flexure Region: 30,000 lb NF load (MSC Nastran)
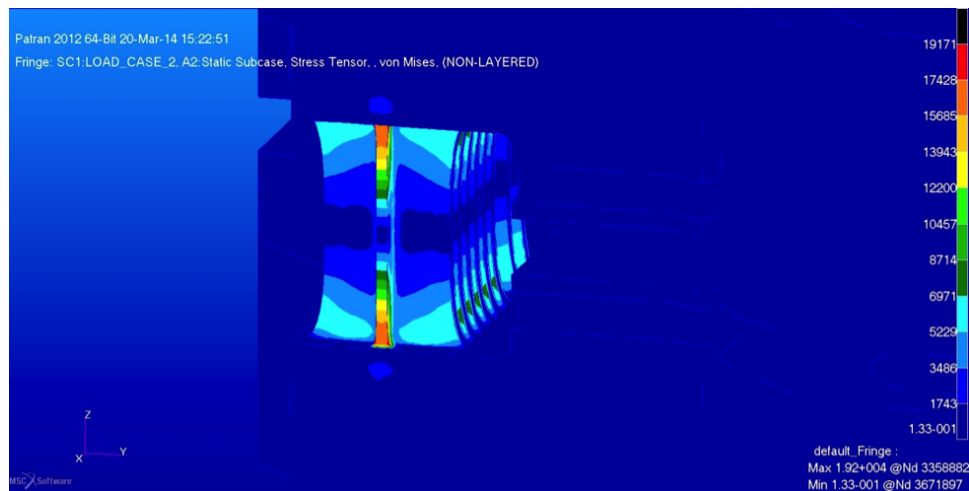
(b) ARC-11-30K Flexure Max. von Mises Stress within Flexure Region: 3,000 lb AF load (MSC Nastran)

Figure 17. Flexure von Mises Stress (Load Cases 1 and 2)

a database program for data analysis. The resulting data are reviewed and then parsed in order to identify the most critically stressed nodes in the balance. These nodes are then be used to compute node stress coefficients, which are essentially the node stresses divided by the computed load. These stress coefficients will be monitored real-time during actual balance use to determine the stress state of the balance for purposes of computing fatigue life cycles.

Measured balance loads during testing have static (0-2 Hz) and dynamic (>2 Hz) components that exist simultaneously. Material fatigue is caused by load cycling due to both components, but the typically dominated by the dynamic cycling at higher frequencies. The Goodman approach from fatigue analysis decomposes the static (low-cycle fatigue) and dynamic (high-cycle fatigue) components that result in a load effect. The Goodman algorithms weigh the static and dynamic components differently and allows for a method where a safe loading boundary condition can be established based on these decomposed signals.

The fatigue cycle counting that is performed is based on knowledge of the Mechanical balance structure, and which areas of the balance are critical based on performing a finite element analysis of the model under specified loading conditions (generally the balance design loads). In order to determine which areas of the balance are deemed critical, a FEA is performed and the worst-case finite element nodes are determined

Table 10. Critical Stress Node Outputs

1. Node ID	11. Coordinate CID	21. Maximum Shear Stress (psi)
2. Node X-Location (in)	12. von Mises Stress (psi)	22. Normal Strain epsilonxx (in/in)
3. Node Y-Location (in)	13. Normal Stress sigmaxx (psi)	23. Normal Strain epsilonyy (in/in)
4. Node Z-Location (in)	14. Normal Stress sigmayy (psi)	24. Normal Strain epsilonzz (in/in)
5. X-Translational Displacement (in)	15. Normal Stress sigmazz (psi)	25. Shear Strain epsilonxy (in/in)
6. Y-Translational Displacement (in)	16. Shear Stress sigmaxy (psi)	26. Shear Strain epsilonyz (in/in)
7. Z-Translational Displacement (in)	17. Shear Stress sigmayz (psi)	27. Shear Strain epsilonxz (in/in)
8. X-Rotational Displacement (rad)	18. Shear Stress sigmaxz (psi)	28. Minimum Principal Strain (in/in)
9. Y-Rotational Displacement (rad)	19. Minimum Principal Stress (psi)	29. Maximum Principal Strain (in/in)
10. Z-Rotational Displacement (rad)	20. Maximum Principal Stress (psi)	30. Maximum Shear Strain (in/in)

based on maximum loading conditions representative of the balance design load limits. After the FEA is performed, the worst-case nodes are examined, and from these nodes one is able to compute stress coefficients that are used to measure the nodal stress values at each critical area based on the computed load from the calibration matrix.

For the case where real-time stress monitoring is employed, during use the computed stresses are recorded and by the use of the rain-flow counting algorithm techniques one can decompose a varying stress signal into periods of stress reversal. The absolute value of the filtered dynamic signal is compared to the magnitude of the steady state signal (stress in this case), and these pairs are plotted on a Modified Goodman diagram. The static/dynamic pairs are measured and then computed for each critical node, and then these pairs are assigned to a respective fatigue count *bin* that is based on where the point for that stress point falls in the 100% Max. Balance Load-truncated, Modified Goodman diagram. (This modified Goodman diagram excludes Goodman's yield criteria limit presuming such is greater than the 100% Max. Balance Load). For every data point collected during testing, the stress pairs are computed and their associated location in the Modified Goodman chart is recorded and the *bin* counter is updated for each data sample. This cycle counting allows the balance user to have a sense of how much of the useable balance life is consumed real-time. The notion of performing this stress load monitoring technique is based on the fact that the balance is considered to have a finite life, and one must count the fatigue cycles in order to determine when that finite life is completely consumed.

For this study six primary load cases are being analyzed, cases 1 through 6 previously listed. For each case the data described in Table 10 will be output to data file, and then read into either a database program or analyzed using a technical computing code. The individual load cases are of primary interest, so that the two to three dozen critical nodes on the perimeter of the balance can be determined for each load case. The criticality of these nodes will be based on the maximum stress state of each as a result of each primary loading. Once each critical node is identified by its maximum stress state, the nodes will be ranked based and tabulated with their coordinate dimensions. Each load case will have two to three dozen critical nodes, therefore there will exist a total of 120 to 180 total nodes for all five load cases. The stress state of each node will be used to derive a stress coefficient that is unique for that nodal coordinate on the balance. Through the use of superposition the worst case nodal stress can then be computed from the individual load cases, and compared to the values from the FEA combined load case. An example of how the nodal stress data will be handled by the facility has previously been presented.[3] For the purpose of this paper the critical stress node data is still being analyzed, therefore no results are prepared to present. The end results will be a tabulated list of nodes that are identified by their balance reference frame coordinates (x, y and z), along with the stress coefficients that the test facility can use to monitor the real-time stress state.

V. Future Work

As a result of this initial work in the area of investigating new fillet geometries for stress concentration reduction, future work is being planned to further investigate different optimization strategies for balance designs. These strategies will include additional numerical and experimental research to further look at a more generic overview of non-circular conical fillets in the flexural regions, as well as investigating complete balance design optimization using response surface methodologies and conventional optimization techniques. Part of this research will include utilizing FEA tools in conjunction with these optimization methods to

optimize the complete balance structural design based on the defined constraints and requirements. These constraints and requirements include volumetric/size constraints, Mechanical loads, total stress state of the instrument under worst case loading scenarios, measurement output of the electrical strain gage sensors, material fatigue, and structural dynamic behavior. Future numerical and physical experiments are being planned, in order to assess different optimization techniques and the scalability of the results.

VI.   Conclusions

The motivation for the work detailed in this paper was based on the need to develop a new NASA semi-span balance with improved flexure design techniques. A critical need was defined for the development of a new semi-span balance, where the stress state of the balance will be monitored real-time at all times during operational use in order to measure its fatigue life. In order to design a balance with the goal of maximizing fatigue life, a study was conducted to determine new flexure fillet geometries that minimize stress concentrations under full-scale design loads.

The information presented reveals the methodical process that was undertaken to research a new new proposed fillet geometry for use on these types of balance transducers. As part of this research the successful demonstration of these new design concepts have been detailed, and the case study discussed reveals the impact on the design of a newly developed semi-span balance. The baseline fillet study research and the analysis of the final instrument reveal the significant improvements that can be achieved with proper design techniques. As a result of this initial work, continued research is being conducted to further develop optimization techniques for use in the design of these types of transducers.

VII.   Acknowledgments

References

[1] "Wind-Tunnel Model Systems Criteria (LPR 1710.15)," Tech. rep., NASA Langley Research Center, January 22, 2009.

[2] Avallone, E. A. and Baumeister III, T., *Marks' Standard Handbook for Mechanical Engineering*, McGraw-Hill Science/Engineering/Math, 1996.

[3] Bennett, H. H., "Wind Tunnel Balance Safety of Flight System," *7th International Symposium on Strain-Gauge Balances*, 2010.

[4] Grenat, G., Bret, J., Clavel, G., and Fetet, T., "Real-Time PC Monitoring of Strain-Gage Balances in ONERA's Large Wind Tunnels Using Finite Element Design Tools," *4th International Symposium on Strain-Gauge Balances*.

[5] Rhew, R. D., Skelley, M. L., Woike, M. R., Bader, J. B., and Marshall, T. J., "Partnership for the Revitalization of National Wind Tunnel Force Measurement Capability," *47th AIAA Aerospace Sciences Meeting and Aerospace Exposition*, No. 2009-1514, AIAA, Orlando, FL, January 2009.

[6] Schijve, J., *Fatigue of Structures and Materials*, Springer, 2009.

[7] AIAA, "Recommended Practice: Calibration and Use of Internal Strain Gage Balances with Application to Wind Tunnel Testing," Tech. Rep. R-091-2003, AIAA, 2003.

[8] Balakrishna, S., "NTF Model Protection System MPSS-II," Tech. rep., NASA Langley Research Center, 1999.

[9] Pilkey and Pilkey, *Stress Concentration Factors*, John Wiley & Sons, New Jersey, 3rd ed., 2008.

[10] Baud, R. V., "Fillet Profiles for Constant Stress," *Product Engineering*, April 1934, pp. 133–134.

[11] Baud, R. V., "Further Development in Photoelasticity," *J.O.S.A. and R.S.I.*, 1929, pp. 422–437.

[12] Berkey, D. C., "Reducing Stress Concentrations with Elliptical Fillets," *Society for Experimental Stress Analysis*, Vol. 1, No. 2, New York, December 1945, pp. 56–60.

[13] Lansard, R., "Fillets Without Stress Concentration," *Society for Experimental Stress Analysis*, Vol. 13, No. 1, Philadelphia, September 1954.

[14] Thum, B. and Bautz, W., "Der Entlastungsubergang: Gunstigste Ausbildung des Uberganges an abgesetzten Wellen u. dg." *Forsch. Ingwes*, Vol. 6, 1934, pp. 269.

[15] Montgomery, D., *Design and Analysis of Experiments*, John Wiley & Sons, New York, 7th ed., 2009.

[16] Myers, R. H. and Montgomery, D. C., *Response Surface Methodology*, John Wiley & Sons, 2nd ed., 2002.

[17] Gere, J. M., *Mechanics of Materials*, Brooks/Cole, Pacific Grove, California, 5th ed., 2001.

[18] Sutton, M. A., Orteu, J., and Schreier, H. W., *Iamge Correlation for Shape, Motion and Deformation Measurements - Basic Concepts, Theory and Applications*, Springer, New York, 1st ed., 2009.